THE E835 JET TARGET UPGRADE
Report on summer '93 tests

D. Allspach, G. Boero, M.Marinelli, E. Robutti

Introduction

The E835 experiment is interested in the collision of an antiproton beam and a hydrogen jet stream to study states of charmonium formed in antiproton-proton annihilations. The main goal of the upgraded experiment is to increase the integral luminosity with respect to the previous E760 set-up: this is accomplished by increasing the density of both the antiproton beam and the hydrogen jet.

We are working on the second point, that is getting a higher target density in the interaction area. In order to reach this result we will:

- lower the initial hydrogen temperature;
- improve the alignment and definition of the hydrogen cluster jet;
- minimize the amount of background gas sent into the Antiproton Accumulator pipe from the Jet Target.

In particular, the last goal can be achieved by choosing operating conditions such as to optimize the ratio of the jet density to the Accumulator background pressure and by improving the Jet Target pumping capacity.

We can estimate the average density of the jet by use of the relation

$$\overline{\rho}_p = \frac{\Phi_p}{A_{\text{jet}} v_{\text{cl}}}, \tag{1}$$

where Φ_p is the flux of protons (= flux of hydrogen atoms), A_{jet} is the average jet cross section in the interaction zone, v_{cl} is the cluster speed (supposed uniform) and $\overline{\rho}_p$ is expressed .in protons/cm^3. So the purpose of our measurements is mainly the determination of all these quantities for different working conditions.

The following is a short report of the tests and measures performed during summer '93, with some discussion about the results obtained. A complete report, with full description of the instrumentation, details on measurements procedures, discussions of problems found and reliability, as well as some fundamental theory arguments, can be found in [1].

The nozzle

The jet is produced by making the hydrogen gas expand through a nozzle into a high vacuum chamber. During the expansion, the H_2 molecules undergo a process of condensation which makes them join together to form big clusters (in our case their size is about 10^4 - 10^5 atoms/cluster, see ref. [2], [3]). A cluster jet is thus formed which constitutes the core of the hydrogen flow (see *fig.* 1) and has the required characteristics of high density and directionality. To isolate it and keep the uncondensed gas from diffusing into the AA pipe, it is then necessary to interpose a number of distinct chambers, connected through skimmers and collimators. This is sketched in *fig.* 2.

Several considerations can be made if we make the assumption that we can treat the process as an adiabatic flow through a converging-diverging nozzle. We then have equations relating pressure, temperature, density and flow speed of the gas in expansion to its stagnation condition and the nozzle geometry (see e.g. [2]). In particular we can find from these the expression of the mass flow:

$$\dot{m} = P_0 A_{\text{th}} \left[\frac{W}{RT_0} \left(\frac{2\gamma}{\gamma+1} \right)^{\frac{\gamma+1}{\gamma-1}} \right]^{\frac{1}{2}}, \tag{2}$$

Fig. 1. Condensation and formation of the cluster jet during gas expansion in a conical nozzle.

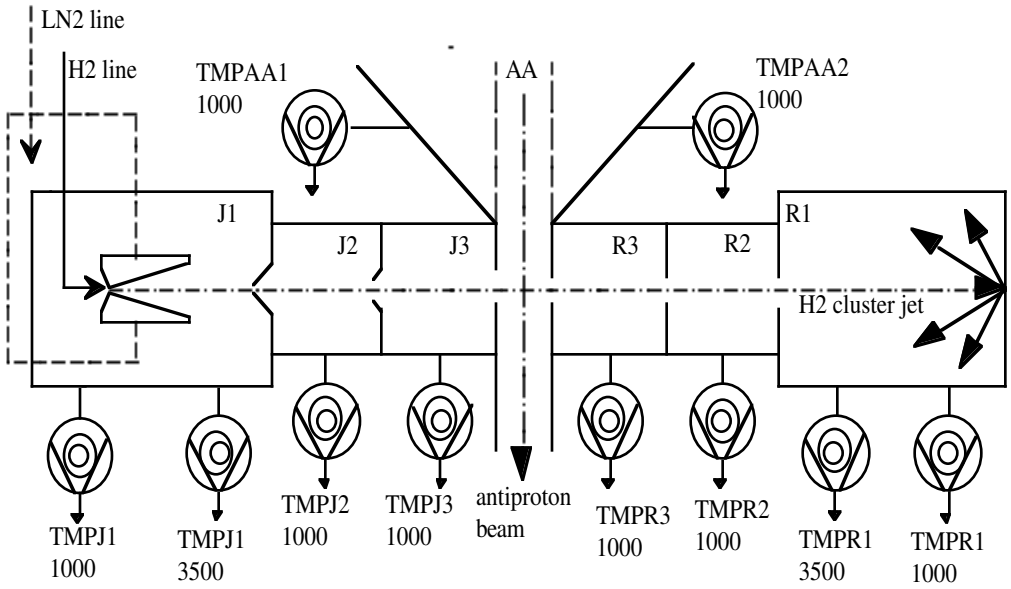

Fig. 2. Schematic of the Jet Target with the differential pumping stages: J1, J2, J3: production stages; R1, R2, R3: sink stages

where P_0 and T_0 are the stagnation pressure and temperature of the hydrogen gas, W its molecular weight, A_{th} the cross section of the nozzle throat and $\gamma = c_P/c_V$. In our case (hydrogen with $\gamma = \frac{5}{3}$ and expansion chamber at $T = 300^{\circ}\text{K}$) this gives an expression for the *throughput* Q:

$$Q[\text{torr}\cdot\text{lit}/\text{sec}] = 8.30\cdot 10^{-3}\,\frac{P_0[\text{bar}]\left(d[\mu\text{m}]\right)^2}{\sqrt{T_0[^{\circ}K]}} \qquad (\text{T} = 300^{\circ}\text{K}), \tag{3}$$

with d the diameter of the nozzle throat. From both (2) and (3) we can argue why we take advantage of decreasing the nozzle (i.e., stagnation) temperature.

The pumping speed in the expansion chamber ($J1$ chamber) sets an upper limit to the amount of gas we can send in. If we keep the throughput fixed at 10 torr·lit/sec (really it is perhaps somewhat lower: see following), we get a constraint on P_0 and T_0 values, which is shown in *fig*. 3 (dashed lines) for three different nozzle diameters). In the same figure the hydrogen vapour pressure curve is also plotted: the working point has to be chosen on the right side of the curve, so as to keep hydrogen in the gaseous phase.

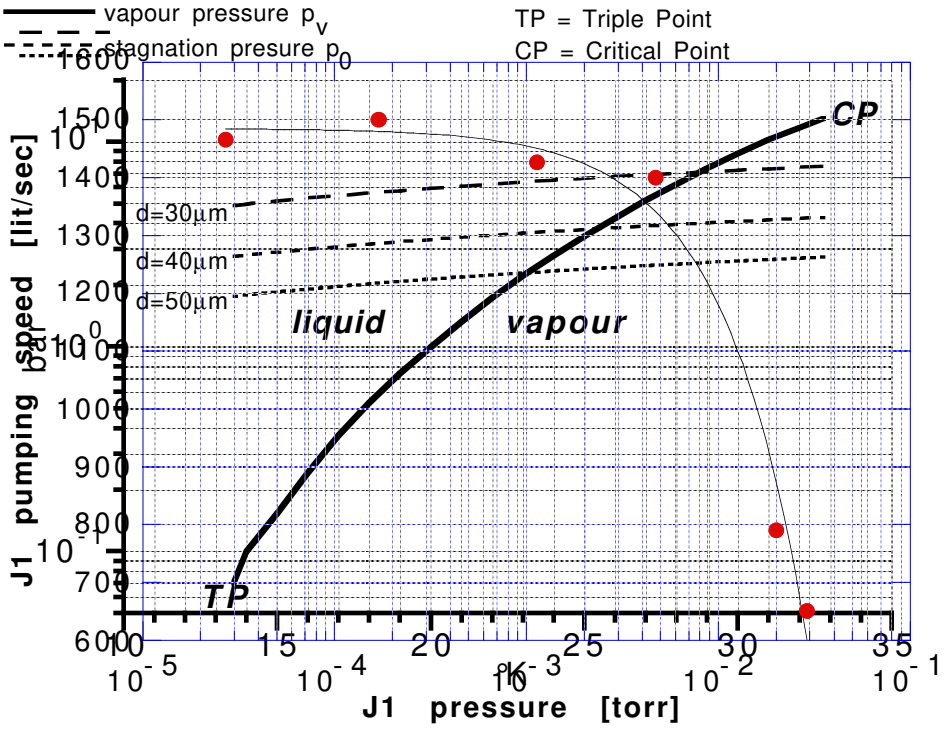

Fig. 3. Vapour pressure curve (solid line) for hydrogen and constant-throughput curves (dashed lines, Q = 10 torr·lit/sec) for three different diameters of the nozzle throat.

Fig. 4. Measured pumping speed in *J*1 chamber as function of *J*1 pressure.

It has been possible to test two different nozzle, both trumpet-shaped but with different throat diameter: 37 μm and 56 μm.

Throughput and background

To evaluate the jet density and the amount of background gas we send into the *AA* pipe, we need to know the hydrogen throughput into the different chambers for various configurations. The *throughput* Q is defined by

$$Q = \frac{\mathrm{d}(PV)}{\mathrm{d}t}, \tag{4}$$

where P and V are the pressure and volume of the chamber where we are making the measurement; it is usually expressed in torr·lit/sec.

In order to measure Q we tried to get a good estimate of the *pumping speed* S for the various chambers of the system: the two quantities are related by

$$S = \frac{Q}{P}. \tag{5}$$

The first necessary operation was the calibration of the vacuum instruments we used for the measure: this is especially important for the ion gauges. The calibration was performed by means of a 'spinning rotor' instrument, by comparing the response of the different types of devices for suitable pressure values (where both could work).

Next, we let a calibrated hydrogen leak (with known throughput) flow separately into the chambers from apposite inlets, measured each time the pressure and got the pumping speed from (5). The values found for J1 chamber are plotted in *fig.* 4 as function of the pressure in the chamber. In *tab.* 1 we report all the measured pumping speeds and conductances.

The pumping speed being known, we could go on measuring the throughput for some particular configurations. This can be expressed in terms of the molecular flux of hydrogen, Φ_{mol} (number of molecules per unit time), as

$$\Phi_{mol} = \frac{Q}{kT}. \tag{6}$$

If we make the assumption that the pumped gas is essentially composed of the H_2 molecules thermalized at 300°K, we then have the correspondence

$$1 \text{ torr} \cdot \text{lit/sec} \rightarrow 3.21 \cdot 10^{19} \text{ mol./sec}. \qquad (T = 300^{\circ}\text{K}) \tag{7}$$

Φ_{mol} is just twice the proton flux in (1).

We are interested in the throughput due to the jet clusters and in that due to the background gas. For this purpose we mounted a metal plaquette on the *density detector* we used for the jet shape measurements (see *fig.* 9): this could be interposed on the jet stream line in *AA* and destroy all the clusters. Then we performed pressure measurement in *AA* and *R*1 chambers with the jet on and freely streaming and with the jet stopped by the plaquette. From the difference between the total (jet stopped) and the background throughput in *AA* we got the cluster jet throughput: the resulting values are plotted in *fig.* 5.

The general behaviour of the total throughput in *R*1 is shown in *fig.* 6 for the two different nozzles. Several considerations can be made about it. After the onset of clusterization (which takes place for the 56 μm nozzle at lower H_2 pressure than for the 37 μm one), the throughput grows linearly with the

Pumping Speed for N_2	**Pumping Speed for H_2**	**Conductance**
S_{J1} = (1180 ± 50) lit/sec	S_{J1} = (1450 ± 100) lit/sec	
	S_{J2} = (650 ± 50) lit/sec	$C_{J1\text{-}J2}$ = 1.7 lit/sec
S_{J3} = (480 ± 20) lit/sec	S_{J3} = (660 ± 50) lit/sec	$C_{J2\text{-}J3}$ = 6.4 lit/sec
S_{AA} = (115 ± 15) lit/sec	S_{AA} = (430 ± 40) lit/sec	$C_{J3\text{-}AA}$ = 22 lit/sec
S_{AA1} = (520 ± 40) lit/sec	S_{R3} = (700 ± 40) lit/sec	$C_{AA\text{-}R3}$ = 40 lit/sec
	S_{R2} = (740 ± 40) lit/sec	$C_{R3\text{-}R2}$ = 100 lit/sec
S_{R1} = (1130 ± 100) lit/sec	S_{R1} = (2350 ± 100) lit/sec	$C_{R2\text{-}R1}$ = 150 lit/sec

Tab. 1 Measured values of the pumping speed and conductance in the different chambers of the Jet Target (the pumping speed depends on the gas being used).

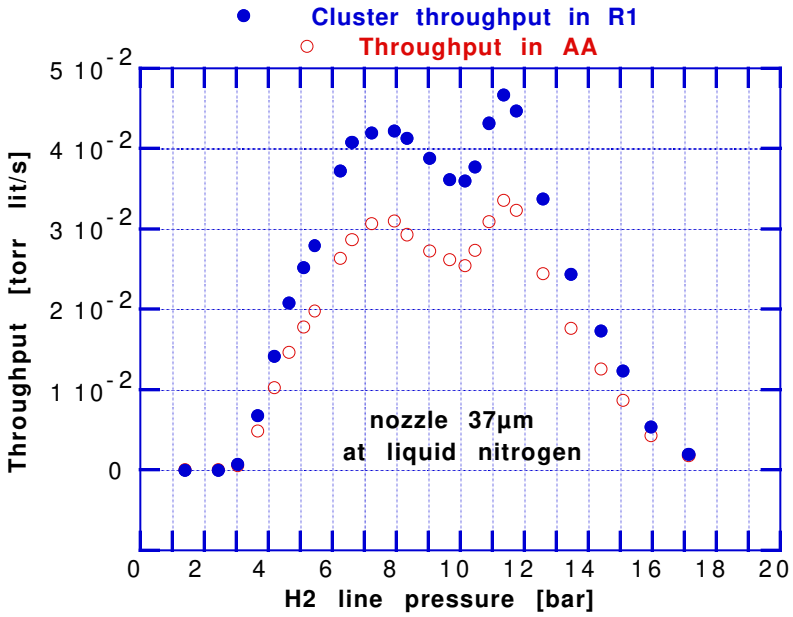

Fig. 5. Cluster throughput as function of P_0. The two sets of data corresponds to the measurements made in *R*1 and *AA*: the difference between them could be due to the different position of the ion gauges with respect to the cluster formation zone.

stagnation pressure. This is in good agreement with the simple theoretic calculation relative to an adiabatic expansion of a perfect, non-viscous gas in continuum flux (solid line in *fig*. 7, showing the throughput in *J*1). Raising the pressure, the throughput shows a maximum (two peaks for the 37 µm nozzle) and then decreases. A reasonable justification could be the increasing amount of gas diffusing in *J*1 chamber and interfering with the jet: the pressure in *J*1 reaches those values for which we observe the decreasing

pumping speed quoted in *fig.* 4. This is clear from *figs.* 8*a*,8*b*. A further increase can be shown to be due

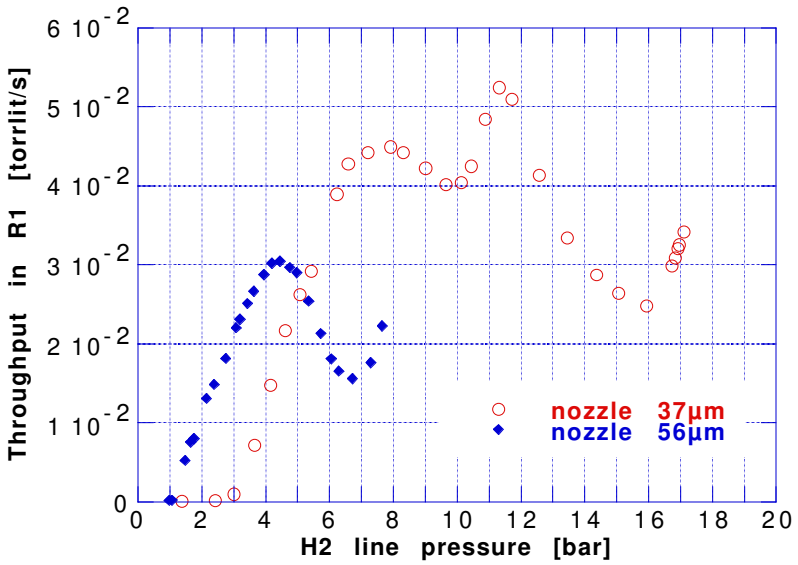

Fig. 6. Throughput in *R*1 for the two different nozzles.

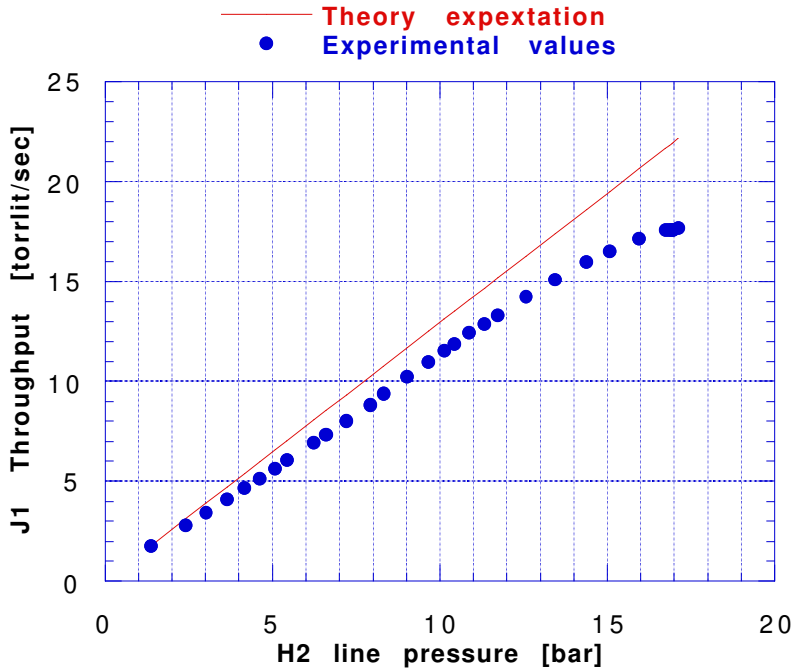

Fig. 7. Measured throughput in *J*1 compared to theory expectations. Solid line is obtained from eq. (3) with T_0 = 800€K, d = 37µm.

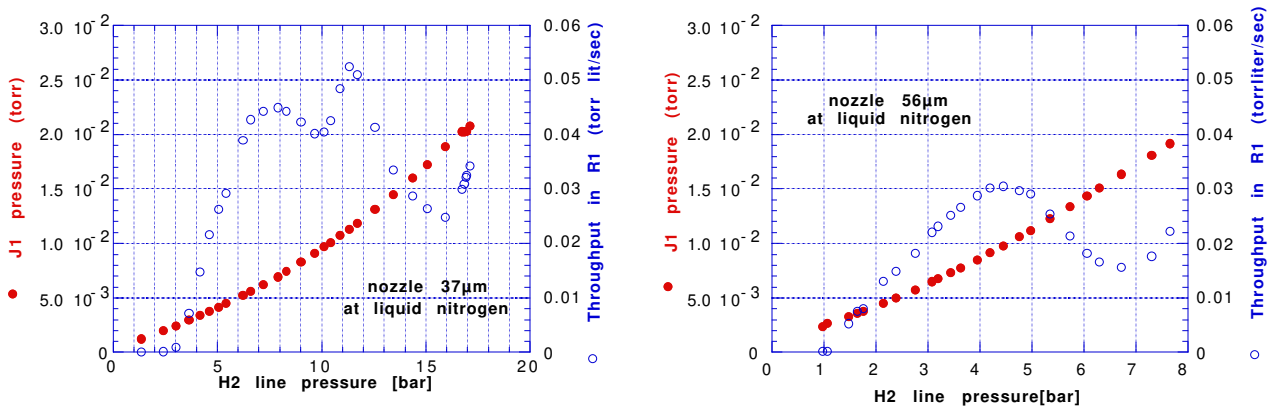

a *b*

Fig. 8. Throughput in *R*1 and *J*1 pressure vs. H_2 line pressure for the two different nozzles. Notice that the throughput decrease begins in correspondace with about the same values for P_{J1} (~ 10^{-2} torr).

to an "effusive throughput", that is, that due to molecules not belonging to the jet and diffusing into *R*1 chamber.

Jet shape

We used a simple method to find the shape of the jet at the intersection point, by which we could estimate the cross section of the jet which appears in (1). The method makes use of a thin needle crossing the jet section and is similar in this to that used formerly in the *E*760 set-up, the only difference being the needle location (inside the AA instead of *R*1 chamber). It is based on the following principle: when the hydrogen clusters hit the needle, they break, or 'evaporate', scattering atoms all around the chamber and causing an increase in pressure. The higher the rate of hits (and so the hydrogen flux), the higher the pressure rise.

To determine the jet shape we need to sweep its cross section in both the *x* and *y* (orthogonal) directions. To accomplish this we fixed an L-shaped needle (see *fig.* 9) at the end of a long arm inserted, perpendicularly to the jet, in the *AA* section. The head supporting the needle is equipped with two kinds of movements, each controlled by a stepping motor: it can be moved back and forth along the *z* axis (thus allowing for horizontal sweep of the vertical needle) or it can rotate around the *z* axis (thus allowing for vertical sweep of the horizontal needle).

Before starting the measure we made sure we had a good alignment of the whole system by checking that the nozzle was right on the *x* axis. This we could make by means of a little glass window inserted in the *R1* wall in front of the nozzle, a telescope, and a lamp placed inside *J1* chamber. To correct for possible misalignment, the nozzle was equipped with *x*-*y* movements (now with angular movements too).

Some results are plotted in *fig.* 10. There are two different plots for the *y*-sweep because the needle can cross the jet for two different *x*-values (*fig.* 11). The exact position of the needle is known within a 0.4 mm error, its diameter being 0.8 mm. Measurements were made with different stagnation pressures, temperatures and nozzle throat diameters: we notice that the jet is centred on the *x* axis to within ~ 0.5 mm, shows approximated cylindrical symmetry and doesn't have large tails on the borders (1 mm inside it the density is more than 80% its maximum).

Cluster speed

Another necessary information we need for the evaluation of the target thickness is the cluster speed. We know from literature (ref. [3],[4]) that this speed shows a distribution with a narrow peak around a well-defined value, so that we can treat the cluster as all having the same velocity.

Fig. 9. The *density detector*, the device used for measuring the geometry and throughput of the cluster jet inside *AA*.

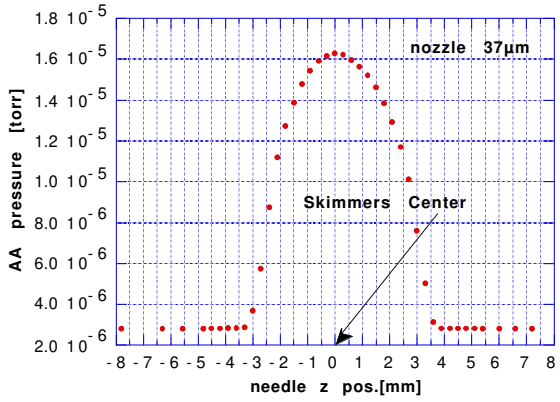

a

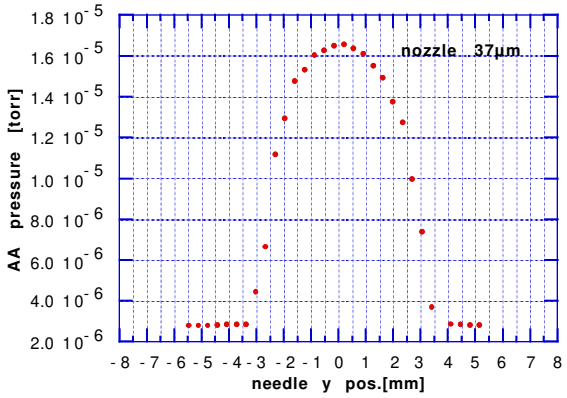

b

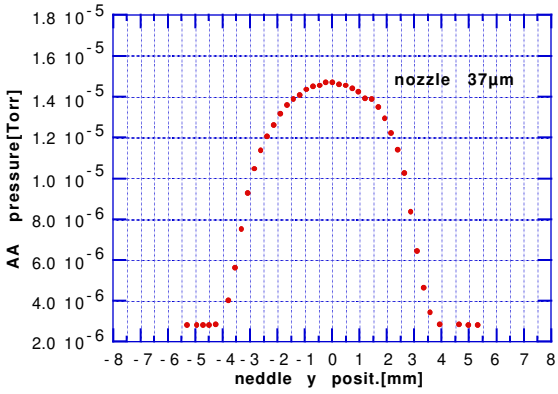

c

Fig. 10. Jet shape plots: *a*) horizontal sweep; *b*) vertical sweep with needle at $x = -19$ mm; *c*) vertical sweep with needle at $x = +19$ mm.

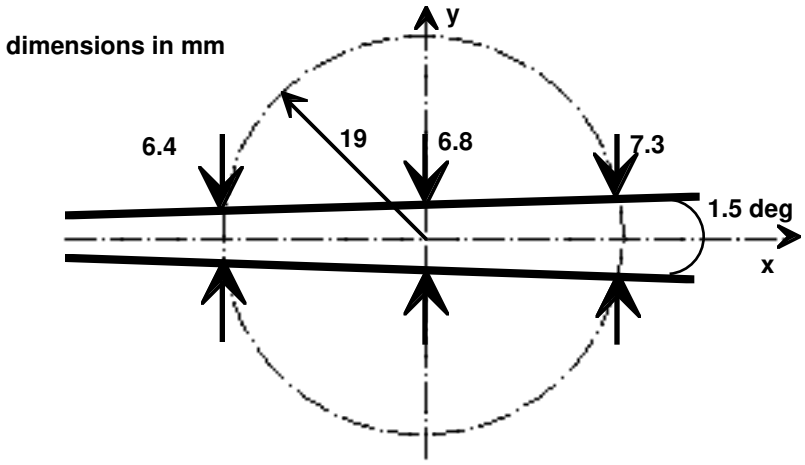

Fig. 11. Jet dimensions in the *AA*: the 19 mm radius circle is that swept by the L-shaped needle when rotating around *z* axis (notice the two intersections with the jet).

For this measure we periodically chopped the jet inside the *AA* pipe and looked downstream (*R*1 chamber) for the propagation of this perturbation, thus measuring the elapsed time in between. The chopper consisted in a rotating metal cylinder with two "¼ period" windows (see *fig.* 12) and axis along the *z* direction; its motor allowed rotation frequencies as high as 400 Hz. The detector was an ion gauge installed in *R*1 just on the jet stream; the overall time response of the electronic used to read it was below 1 μsec.

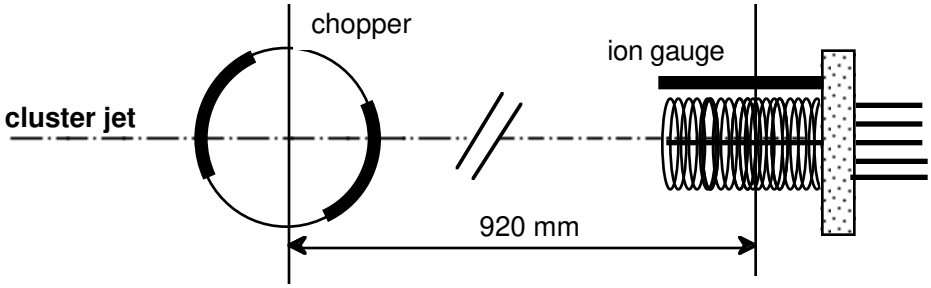

Fig. 12. Schematic of the set-up for the cluster speed measurement: the chopper is inside *AA* and the detector (ion gauge) inside *R*1.

What we read on the oscilloscope was the phase difference between the chopper and the signal of the ion gauge: we got the copper phase by means of another thin slit on the cylinder that periodically passed between a LED and a phototransistor (both fixed). We have the relation

$$\Delta\phi = 2\pi(2\nu)t_f + c\,, \tag{8}$$

where $\Delta\phi$ is the phase difference, 2ν the chopping frequency (= twice the rotation frequency), t_f the *time of flight*, and c a constant depending on the trigger locked to the chopper. So we have a linear relation between $\Delta\phi$ and ν and, by repeating the measure for different values of ν we can extract t_f as

$$t_f = \frac{1}{2}\frac{1}{2\pi}\frac{\mathrm{d}(\Delta\phi)}{\mathrm{d}\nu} \tag{9}$$

(*fig.* 13). Knowing the distance between chopper and detector, d = 920 mm, we could thus get v_{cl}.

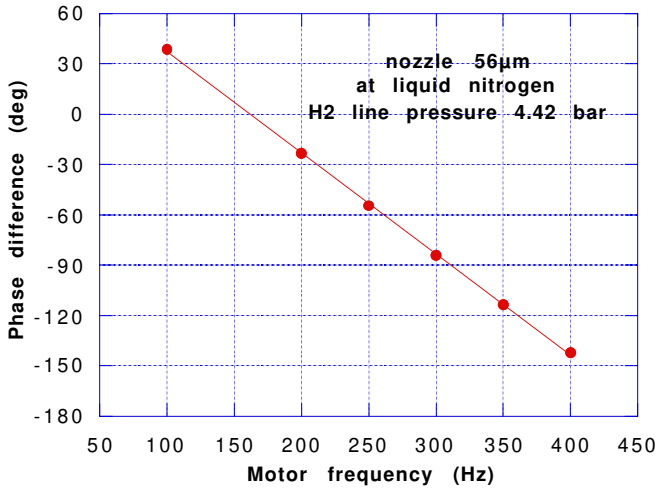

Fig. 13. Measured phase difference between signal in *R*1 and chopper, as function of the chopper rotation frequency.

For this measurement we used a lock-in amplifier. The values found for v_{cl} are plotted in *fig.* 14 as function of the H_2 line pressure, together with the rms signal detected, and are in good agreement with theoretic estimates.

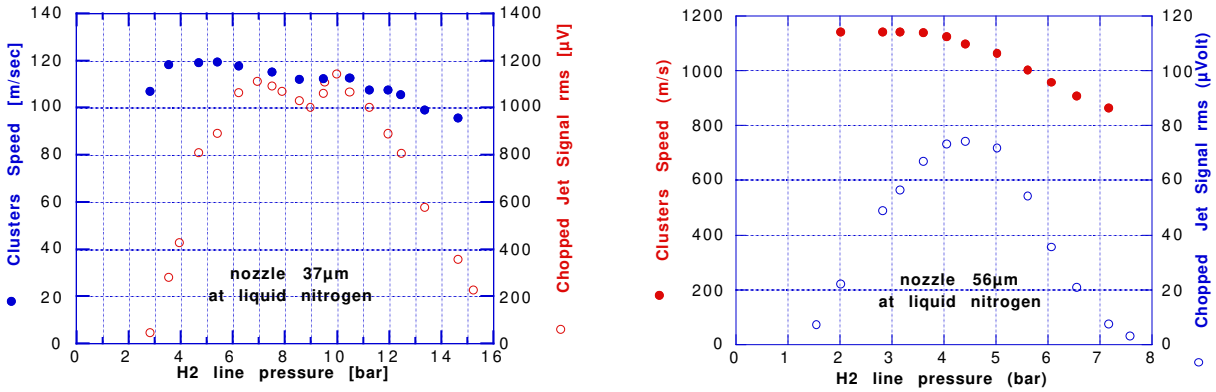

a *b*

Fig. 14. Measured cluster speed and rms signal in *R*1: *a*) for the 37 μm nozzle; *a*) for the 56 μm nozzle.

Conclusions and hints

Having determined the preceding jet parameters, we could be able to evaluate its average density by the use of eq. (1). The resulting jet densities at different H_2 line pressures are plotted in *fig.* 15 and show a structure similar to that of the jet throughput (v_{cl} varies little in that range of pressure).

The *target thickness* is expressed as

$$\hat{\rho}_p = \Delta z(x,y) \cdot \rho_p, \tag{10}$$

where $\Delta z(x,y)$ is the length occupied by the jet for given x and y co-ordinates. At the centre of the jet it is therefore of the order of 10^{13} protons/cm^2 ($1 \div 5 \cdot 10^{13}$ p/cm^2). Unfortunately these values are of the same order of magnitude of the thickness of the background gas near the jet and in the rest of the *AA* pipe. For $P_0 = 7$ bar, for example, we estimated both of them to be ~ 10^{13} p/cm^2, while $\hat{\rho}_p = 4 \cdot 10^{13}$ p/cm^2 (with the

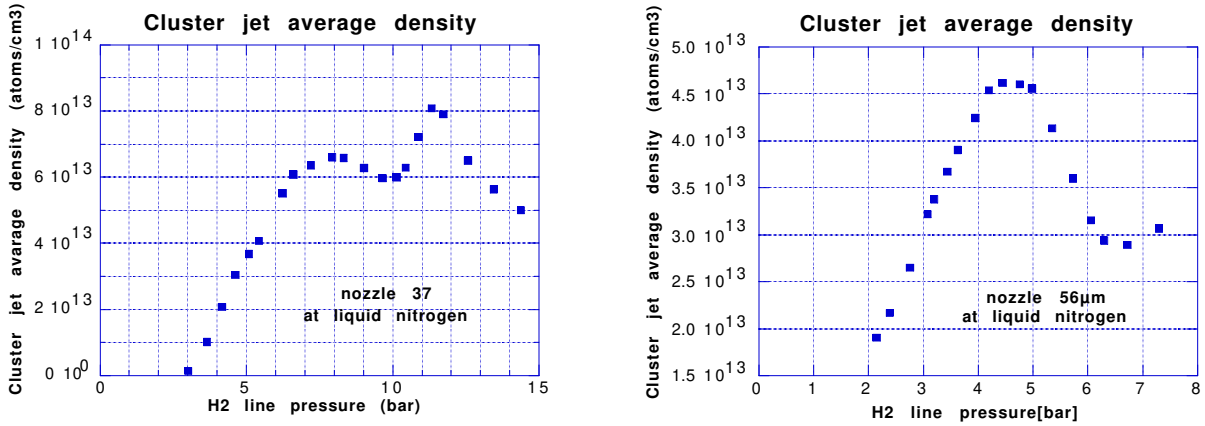

a *b*

Fig. 15 The jet average density calculated from (1) and measured data: *a*) for the 37 μm nozzle; *b*) for the 56 μm nozzle;

37 μm nozzle). As the background grows with P_0, it's not useful to set the H_2 line pressure to its maximum (thus raising the jet density), if this shortens too much the antiproton beam lifetime. We defined a 'jet target efficiency' *JTE*,

$$JTE = \frac{\hat{\rho}_p}{\hat{\rho}_{\text{back}}}; \tag{11}$$

an estimate of this quantity is the ratio $\left(Q_{\text{cl}}^{(R1)} / Q_{\text{back}}^{(R1)}\right)$ (cluster to background throughput in *R*1), which we can evaluate directly. This is plotted in *fig.* 18 for the 37 μm nozzle. From there we can see that the highest efficiency does not coincide with the highest jet density, and suggests we should work at lower pressure than we could argue from the density behaviour alone.

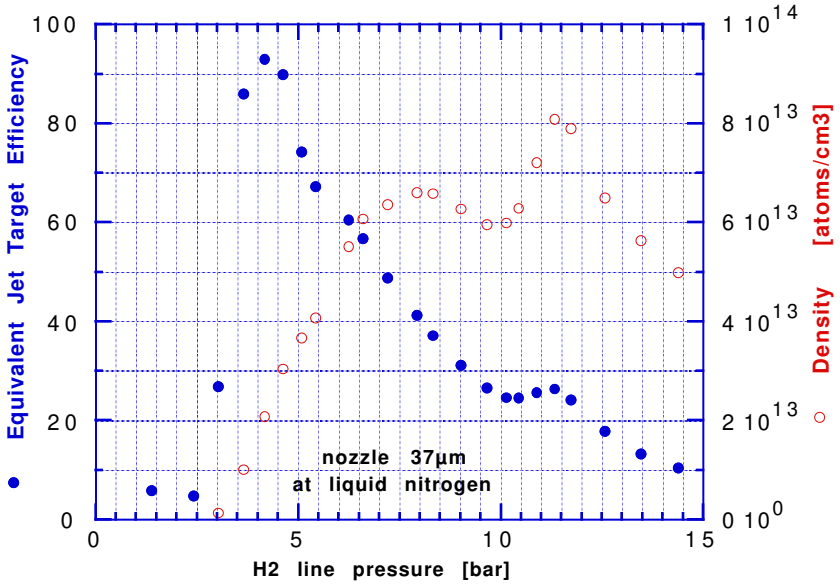

Fig. 16. An estimate of the *Jet Target Efficiency* using the ratio $Q_{\text{cl}}^{(R1)} / Q_{\text{back}}^{(R1)}$.

A useful upgrade would be that of adding two getter pumps in the Antiproton Accumulator adjacent to the Jet Target, upstream. In fact we have there a region of approximately 2 m between the *AA*1 and *AA*2 turbomolecular pumps (close to the target) and the nearest ion pump in the beam pipe. That section of pipe has a conductance of about 100 lit/sec: as the total pumping speed of the interaction area is 1400 lit/sec, we have consequently a throughput into the beam pipe which amounts to $\frac{1}{14}$ of the background throughput. In typical working conditions this is about 1000 torr·lit/sec: by use of (1), (5), (6), (10) (with a length of the interaction area of 2 m) this corresponds to a thickness

$$\hat{\rho}_{\text{interaction}} \approx 10^{13}\,\text{protons} / \text{cm}^2. \tag{12}$$

Similarly, for the upstream region we find

$$\hat{\rho}_{\text{upstream}} \approx 10^{13}\,\text{protons} / \text{cm}^2, \tag{13}$$

so that they are roughly the same. It is then evident the usefulness of having a higher pumping speed upstream of the interaction zone to keep a longer life of the antiproton beam.

Finally we want to note that we have the possibility of keeping constant the luminosity of the experiment throughout the run. This is possible by continually monitoring the rate of events (by the

luminosity monitor) and using it as a feedback for the H_2 line pressure: as the antiproton beam intensity decreases, we gradually raise the pressure and so the jet density (target thickness).

References

[1] G. Boero, *graduation thesis*, 1994

[2] O. F. Hagena, W. Obert, *J. Chem. Phys*, **56**, 1793 (1972)
[3] J. Gspann, K. Körting, *J. Chem. Phys.*, **59**, 4726 (1973)
[4] E. Becker, *Gas Dynamics*, Academic Press, New York